

Molecular Characterization of the Pediatric Preclinical Testing Panel

Geoffrey Neale,¹ Xiaoping Su,¹ Christopher L. Morton,² Doris Phelps,² Richard Gorlick,⁶ Richard B. Lock,⁷ C. Patrick Reynolds,⁸ John M. Maris,¹¹ Henry S. Friedman,¹² Jeffrey Dome,³ Joseph Khoury,⁴ Timothy J. Triche,⁹ Robert C. Seeger,¹⁰ Richard Gilbertson,⁵ Javed Khan,¹³ Malcolm A. Smith,¹⁴ and Peter J. Houghton²

Abstract Purpose: Identifying novel therapeutic agents for the treatment of childhood cancers requires preclinical models that recapitulate the molecular characteristics of their respective clinical histotypes.

Experimental Design and Results: Here, we have applied Affymetrix HG-U133Plus2 profiling to an expanded panel of models in the Pediatric Preclinical Testing Program. Profiling led to exclusion of two tumor lines that were of mouse origin and five osteosarcoma lines that did not cluster with human or xenograft osteosarcoma samples. We compared expression profiles of the remaining 87 models with profiles from 112 clinical samples representing the same histologies and show that model tumors cluster with the appropriate clinical histotype, once “immunosurveillance” genes (contributed by infiltrating immune cells in clinical samples) are eliminated from the analysis. Analysis of copy number alterations using the Affymetrix 100K single nucleotide polymorphism GeneChip showed that the models have similar copy number alterations to their clinical counterparts. Several consistent copy number changes not reported previously were found (e.g., gain at 22q11.21 that was observed in 5 of 7 glioblastoma samples, loss at 16q22.3 that was observed in 5 of 9 Ewing’s sarcoma and 4 of 12 rhabdomyosarcoma models, and amplification of 21q22.3 that was observed in 5 of 7 osteosarcoma models). We then asked whether changes in copy number were reflected by coordinate changes in gene expression. We identified 493 copy number – altered genes that are nonrandom and appear to identify histotype-specific programs of genetic alterations.

Conclusions: These data indicate that the preclinical models accurately recapitulate expression profiles and genetic alterations common to childhood cancer, supporting their value in drug development.

Authors’ Affiliations: ¹Hartwell Center of Bioinformatics and Biotechnology and Departments of ²Molecular Pharmacology, ³Oncology, ⁴Pathology, and ⁵Developmental Neurobiology, St. Jude Children’s Research Hospital, Memphis, Tennessee; ⁶Albert Einstein College of Medicine, The Children’s Hospital at Montefiore, Bronx, New York; ⁷Children’s Cancer Institute Australia for Medical Research, Randwick, New South Wales, Australia; ⁸Children’s Hospital of Los Angeles; ⁹Department of Pathology and Laboratory Medicine and ¹⁰Division of Hematology-Oncology, Children’s Hospital, Los Angeles, California; ¹¹Children’s Hospital of Philadelphia, University of Pennsylvania School of Medicine and Abramson Family Cancer Research Institute, Philadelphia, Pennsylvania; ¹²Duke University Medical Center, Durham, North Carolina; and ¹³Oncogenomics Section, Pediatric Oncology Branch and ¹⁴Cancer Therapy Evaluation Program, National Cancer Institute, NIH, Bethesda, Maryland

Received 12/7/07; revised 2/22/08; accepted 3/1/08.

Grant support: National Cancer Institute grant NO1-CM-37027-23.

The costs of publication of this article were defrayed in part by the payment of page charges. This article must therefore be hereby marked *advertisement* in accordance with 18 U.S.C. Section 1734 solely to indicate this fact.

Note: Supplementary data for this article are available at Clinical Cancer Research Online (<http://clincancerres.aacrjournals.org/>).

Requests for reprints: Peter J. Houghton, Department of Molecular Pharmacology, St. Jude Children’s Research Hospital, 332 North Lauderdale St., Memphis, TN 38105. Phone: 901-495-3463; Fax 901-495-4290; E-mail: peter.houghton@stjude.org.

©2008 American Association for Cancer Research.
doi:10.1158/1078-0432.CCR-07-5090

Development of new cancer therapies for children presents certain challenges unique to this population. The incidence of pediatric cancer is relatively low in the United States (1), and multimodality therapy comprising surgery, radiation therapy, and intensive chemotherapy has resulted in overall 5-year survival rates for children with cancer approaching 80% (1). The combination of low incidence and increasingly effective primary therapy results in relatively few children eligible for the evaluation of experimental therapies, and those that are available have generally been extensively treated and have highly resistant disease.

As an approach to overcoming the limitations in childhood cancer drug development noted above, several groups within the pediatric cancer community have systematically tested the validity of preclinical human tumor xenograft models to identify novel agents that may have clinical activity in childhood cancers (2–17). Based on these experiences, the National Cancer Institute has implemented a new initiative, the Pediatric Preclinical Testing Program (PPTP), comprising a consortium of investigators to evaluate new agents *in vitro* and *in vivo*.

For childhood cancers, xenograft models have been quite accurate in identifying clinically active agents and effective drug

combinations particularly when differences in drug exposure between tested animals and humans are taken into account (18). However, the utility of human tumor xenografts in accurately predicting clinical efficacy has been challenged. Concerns raised about xenografts as models for human cancers include (a) the models may not recapitulate the compound genetics of human cancer, (b) the number of models studied per histotype may not represent the heterogeneity likely encountered clinically, and (c) the characteristics of human cancers may change when they are heterografted into immunodeficient hosts in part as a result of the tumor stromal elements being of murine origin. To begin to address these issues in the PPTP, we screened available cell lines and xenografts using cDNA profiling and compared expression profiles with a similar number of clinical biopsies from the same histologies (19). The xenograft models and cell lines quite accurately recapitulated the expression profiles of their respective clinical histologies.

The goal of the present study was to characterize the PPTP panel using whole genome analytic methods: gene expression profiling and whole-genome copy number analyses. These profiles were used to characterize the PPTP samples both within the panel itself and within the context of profiles obtained from primary tumors. Overall, molecular analyses indicate the PPTP *in vitro* and *in vivo* panels represent robust models of their corresponding primary tumor samples.

Materials and Methods

Cell line and xenograft samples. The characteristics of each cell line ($n = 24$) and human tumor xenograft ($n = 63$) have been reported previously (20). Tumor designation and histotype are given in Supplementary Table S1.

Clinical samples. Wilms' tumor and osteosarcoma samples were obtained with institutional review board approval from St. Jude Tissue Bank. Expression data for other tumor histotypes were either from previously published reports (leukemia, ependymoma, and medulloblastoma; refs. 21–23) or from Timothy Triche (Children's Hospital of Los Angeles; Ewing's sarcoma and rhabdomyosarcoma) or from Robert Seeger (Children's Hospital of Los Angeles; neuroblastoma). The distribution of clinical samples and PPTP models according to histotype is shown in Supplementary Table S2.

Gene expression analysis by microarray. Total RNA was prepared from snap-frozen s.c. grown tumor xenografts and patient tumor samples using the RNeasy kit (Qiagen). Gene expression analysis was done in the Hartwell Center Core Laboratory using the Affymetrix HG-U133Plus2 GeneChip (54,613 probe sets). RNA quality was confirmed by UV spectrophotometry and by analysis on the Agilent 2100 Bioanalyzer. Processing of RNA samples was done according to the Affymetrix gene expression protocol. Expression signals were calculated using the MAS5 statistical algorithm within the Affymetrix GCOS software (version 1.4). Signal values were scaled using the global normalization method with the 2% trimmed mean set to 500. Detection calls for each transcript (absent, marginal, or present) were determined using the default variables within the GCOS software.

Analysis of expression data within the PPTP panel was done using \log_2 -transformed signal values where the minimum \log_2 signal was set to zero. For analysis of data originating from different Affymetrix GeneChip (HG-U133A and HG-U133Plus2 microarrays), signal values from the common HG-U133A probe sets (22,215 total) were scaled to a trimmed mean of 500 and then \log_2 -transformed and truncated to a minimum value of zero as described above. The transformed signals were median scaled, and each probe set was individually fitted using a linear model to adjust for chip type.

Principal components analysis and unsupervised hierarchical clustering were done using GeneMaths XT software version 1.6 (Applied Maths). For clustering, the similarity between expression profiles or samples was calculated using the Pearson product-moment correlation coefficient; linkage was calculated using the unweighted pair group method with arithmetic mean.

Analysis of differential expression between tumors and xenografts was done using data collected on the HG-U133Plus2 microarray. GCOS signal values were \log_2 -transformed as described above. Only probe sets with at least one "present" call across the three histotypes (rhabdomyosarcoma, Ewing's sarcoma, and osteosarcoma) were tested. Within each histotype, a t test was done to compare the mean expression of each probe set between primary and xenograft samples. To adjust for multiple-hypothesis testing, the false discovery rate was estimated as described (24). To capture probe sets differentially expressed across histotype, we set a threshold of ≥ 2 -fold difference in expression plus a false discovery rate < 0.0167 in each t test. This threshold corresponded to t test P values of 0.00465, 0.00333, and 0.00352 in the rhabdomyosarcoma, Ewing's sarcoma, and osteosarcoma histotypes, respectively.

Single nucleotide polymorphism analysis by microarray. DNA was extracted from xenograft and tumor samples using DNeasy Tissue kit (Qiagen). Single nucleotide polymorphism (SNP) analysis was done in the Hartwell Center Core Laboratory using the Affymetrix GeneChip Human Mapping 100K assay (116,204 total probe sets). Purity and integrity of DNA samples was confirmed by UV spectrophotometry and by agarose gel electrophoresis. Processing of DNA samples was done according to the Affymetrix 100K SNP protocol.¹⁵ Genotype calls were generated using the dynamic mapping algorithm of the Affymetrix GTYPE software (version 4.0). High-quality SNP array data were obtained for 86 of the 87 PPTP samples (SNP genotype call rates, $\geq 95\%$). Despite repeated attempts, PPTP sample acute lymphoblastic leukemia-2 did not perform well (SNP genotype call rates, $\sim 40\%$) and was excluded from subsequent SNP array analyses.

DNA copy number analyses were done in dChipSNP (25) using the dChipSNP normalization and model-based expression algorithms. Affymetrix CEL files containing probe intensity data were imported into dChip and each array was normalized to a baseline array with median signal intensity using the "invariant set" model (26). Model-based expression was done using the perfect-match/mismatch model to summarize signal intensities for each probe set. For copy number inference, raw (uninferred) copy number was calculated by comparing the signal intensity of each SNP probe set for each tumor sample against a diploid reference set comprising 126 samples (41 Affymetrix public samples, 49 St. Jude Children's Research Hospital acute myelogenous leukemia remission samples, and 36 St. Jude Children's Research Hospital acute lymphoblastic leukemia remission samples). The Hidden Markov Model in dChipSNP was used to infer copy number and to identify genomic amplifications and deletions. Genomic amplifications and deletions were defined by regions containing SNP with inferred copy number of ≥ 3.0 or ≤ 1.0 , respectively. Copy number summary plots according to xenograft histotype were generated by dChipSNP after Hidden Markov Model analysis.

Correlation analysis of gene expression and genomic copy number variation in the PPTP panel. The genomic locations of the HG-U133Plus2 probe sets and the 100K SNP probe sets were obtained from Affymetrix annotations. To identify SNP proximal to an expression probe set, we applied a 50-kb window on either side of the expression probe set. If a SNP was within 50 kb upstream or 50 kb downstream from an expression probe set, that SNP was matched to the expression probe set in subsequent analyses. For expression probe sets interrogating RefSeq transcripts, we applied a special rule. We replaced the original probe set coordinates with those from the RefSeq transcript. The goal was to capture SNP within 50 kb 5' or 3' to the RefSeq

¹⁵ <http://www.affymetrix.com/support/downloads/manuals/100kmanual.pdf>

transcript. After applying these rules to identify "proximal" SNP, we examined the association between genomic copy number and gene expression by linear regression. We fitted a linear regression model of SNP (\log_2 ratio) against expression (\log_2 signal) to estimate the fraction (R^2) of all variations measured in expression among the 86 tumors attributable to underlying DNA copy number alteration. Expression probe sets on the X and Y chromosomes were excluded from the analysis as well as those called "absent" across all PPTP samples or without proximal SNP. Overall, 38,716 of the HG-U133Plus2 probe sets and 77,862 SNP were included in the analysis. Because the majority of expression probe sets had multiple proximal SNP, the SNP with the highest correlation (R^2) value was selected for subsequent analyses.

Results

Characterization within the PPTP panel by gene expression profiling. Previously, we reported the similarity between

expression profiles of childhood cancer models (cell lines and xenografts) and their respective clinical counterparts for selected histotypes as determined by cDNA profiling (19). However, differences in expression profiles are apparent when different platforms are used. As most published reports have used Affymetrix technology, we were interested in determining whether the correlation between expression in models and biopsy samples of childhood cancers was maintained using this technology in which an increased number of genes was probed. We examined both tumor models studied in the cDNA profiling project and additional models that were made available. This analysis showed Rh1 (rhabdomyosarcoma) and SK-NEP (anaplastic Wilms' tumor) to cluster with Ewing's sarcoma models (27). Two brain tumor xenografts in the original cDNA profiling report were determined to be non-human (BT-31 and BT-32, presumably mouse tumors), and the

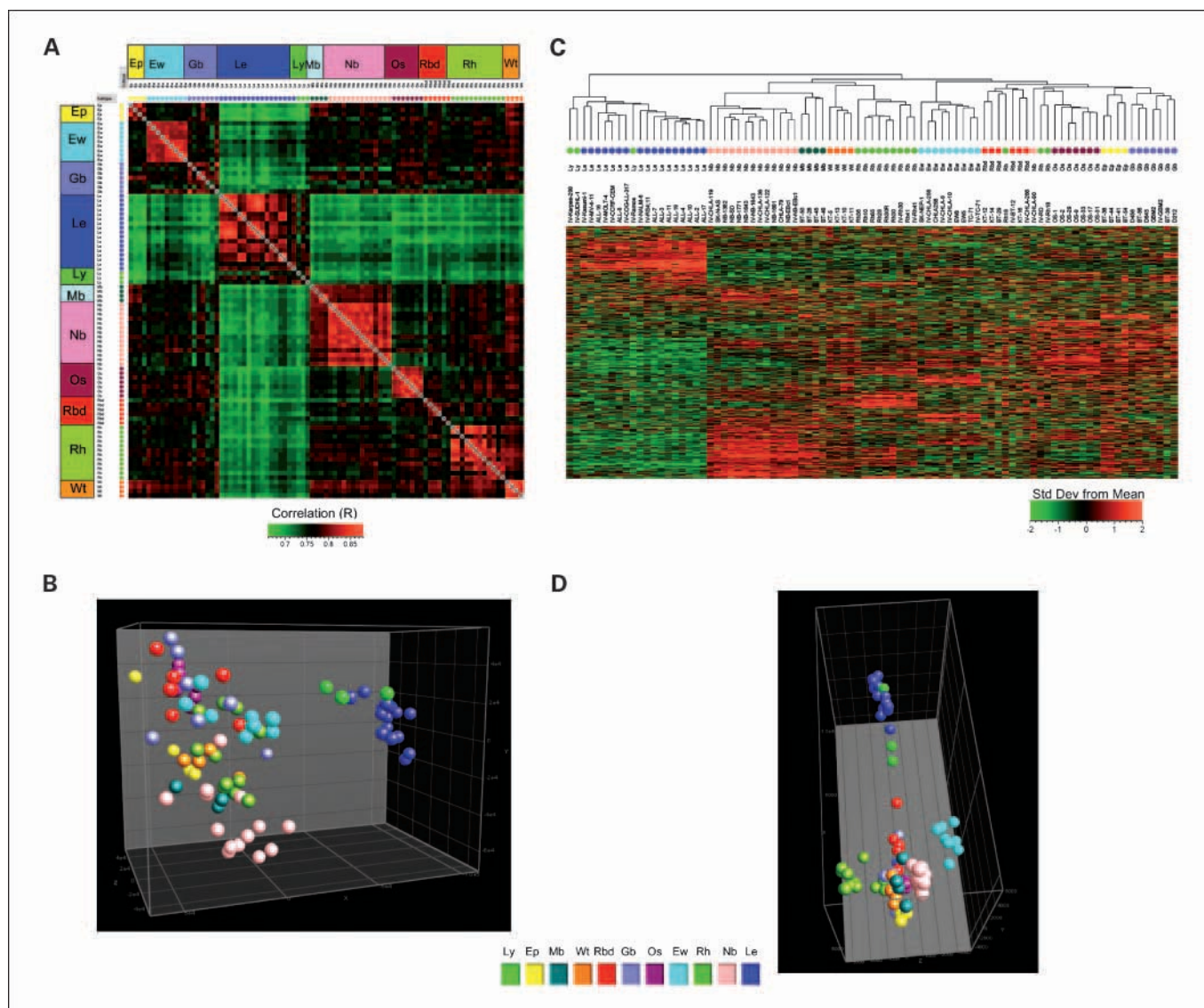


Fig. 1. Expression profile analyses within the PPTP. *A*, pair-wise comparisons of expression profiles (all probe sets) using Pearson's correlation (R) test. *B*, analysis of expression variance using all probe sets by principal components analysis. Each sample is represented by a sphere plotted in three-dimensional space and colored by tumor histotype. *C*, hierarchical cluster analysis of PPTP samples using 2,808 expression profiles with robust variable expression (median absolute deviation >1.6 with at least one "present" call). *X axis*, samples; *Y axis*, gene expression profiles; *colored circles*, histotypes. Heat map colors show overexpressed transcripts (*red*) and underexpressed transcripts (*green*). The scale bar indicates relative expression as SD from the mean. *D*, analysis of expression variance using 2,808 profiles by principal components analysis. Each sample is represented by a sphere plotted in three-dimensional space and colored by tumor histotype.

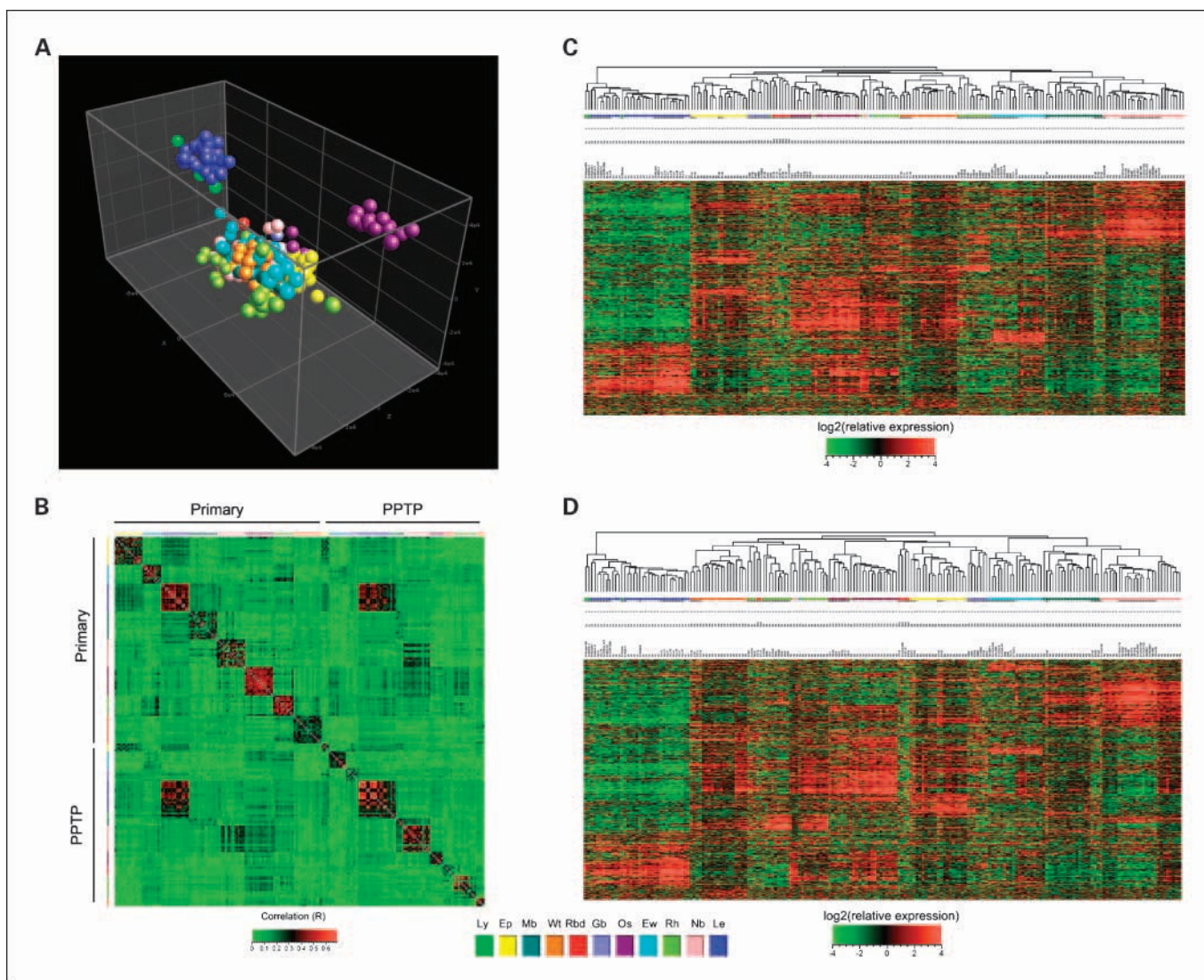


Fig. 2. Expression profile analyses of PPTP and primary tumor samples. *A*, ANOVA (all probe sets) by principal components analysis. Each sample (87 models and 111 primary tumors) is represented by a sphere plotted in three-dimensional space and colored by tumor histotype. *B*, pair-wise comparisons of expression profiles (all probe sets) using Pearson's (R) correlation test. *C*, hierarchical cluster analysis of PPTP and primary tumor samples using 1,695 expression profiles with robust variable expression (median absolute deviation >1.3 with at least one "present" call). *X axis*, samples; *Y axis*, gene expression profiles; *colored circles*, histotypes. Xenografts are further colored with dark shadows. Heat map colors show overexpressed transcripts (*red*) and underexpressed transcripts (*green*). The scale bar indicates relative expression of transcripts using a \log_2 -transformed scale. *D*, hierarchical cluster analysis of PPTP and primary tumor samples using 1,506 expression profiles excluding 135 genes associated with immunosurveillance. *X axis*, samples; *Y axis*, gene expression profiles; *colored circles*, histotypes. Xenografts are further colored with dark shadows. Heat map colors show overexpressed transcripts (*red*) and underexpressed transcripts (*green*). The scale bar indicates relative expression of transcripts using a \log_2 -transformed scale.

profiles from five osteosarcoma cell lines (OS160, OS164, OS166, and OS187) were distinct from either clinical osteosarcoma or other osteosarcoma models in the PPTP panel. These tumors and cell lines were excluded from further experimentation.

We used gene expression profiles generated from the Affymetrix HU-U133Plus2 arrays to identify potential molecular subtypes within the remaining 87 PPTP samples of xenografts and cell lines (Supplementary Table S3; ref. 28). Pair-wise comparison using all 54,613 transcript measurements showed strongest correlation among samples from the same histotype group. The highest correlations of expression were observed within the Ewing's sarcoma, leukemia, neuroblastoma, osteosarcoma, rhabdomyosarcoma, and Wilms' tumor histotype groups (Fig. 1A). Principal components analysis indicated

the major source of variance in gene expression was associated with sample histotype. The greatest difference in profiles was between lymphoid and nonlymphoid histotypes (Fig. 1B). To further explore relationships among the PPTP samples, we selected a subset of transcripts with robust expression variation. Hierarchical clustering using the 2,808 highly variable transcripts confirmed the major separation between leukemic and nonleukemic histotypes (Fig. 1C). Further, these profiles separated the PPTP panel into discrete clusters whose members were almost exclusively based on xenograft and cell line histotype. With three exceptions, all PPTP models clustered according to histotype. The exceptions were in the rhabdomyosarcoma panel [Rh18 (xenograft), IV-Rh18 (*in vitro*), and IV-RD (*in vitro*)] and the neuroblastoma panel [IV-CHLA-90 (*in vitro*)]. Principal components analysis using the 2,808

highly variable transcripts confirmed the separate populations within the PPTP samples. In particular, lymphoid, Ewing's sarcoma, neuroblastoma, and osteosarcoma subtypes were the most distinct (Fig. 1D). Gene Ontology analysis of the highly variable transcripts (Supplementary Table S2) showed significant enrichment of genes involved in tissue specification, especially those involved in neurogenesis and muscle development.

Characterization of the PPTP panel by comparison with the expression profiles of primary tumors. We extended the expression analyses to include gene profiles measured in 111 primary tumors and the PPTP models (Supplementary Table S3). Because some expression measures originated from different Affymetrix GeneChip, we adjusted the combined tumor and xenograft data set according to chip type (see Methods).

The major source of variance in expression was related to tumor histotype. In particular, the lymphoid and osteosarcoma histotypes were the most distinct (Fig. 2A). Pair-wise comparisons of expression profiles indicated greatest similarity within samples from the same histotype (Fig. 2B). The best agreement between xenograft and tumor samples was found in the lymphoid, neuroblastoma, and ependymoma histotypes (Fig. 2B).

Hierarchical clustering was done using a subset of 1,695 transcripts with robust variable expression (Fig. 2C). As observed in the cluster analysis within the PPTP samples, the most significant separation was due to lymphoid versus nonlymphoid histotype. Although there was generally clustering of preclinical models with their clinical counterparts, this was not the case for the rhabdomyosarcoma models. If only profiles from solid tumors were used, all models segregated accurately with the appropriate clinical histotype (with the three exceptions mentioned previously; data not shown). After removal of 135 immunosurveillance profiles from those depicted in Fig. 2C, all PPTP samples clustered with the appropriate clinical histotype (Fig. 2D), including the rhabdomyosarcoma models with the exception of Rh18 and IV-RD. These findings suggested the main distinction between rhabdomyosarcoma tumors and preclinical models was related to expression of immune-related genes. Overall, however, the profiles of the xenograft models most closely resemble their respective primary tumors and recapitulate expression of genes that discriminate between tumor histotypes. In support of this notion, Gene Ontology analysis of the highly variable transcripts showed significant enrichment of genes associated with cell differentiation, cell motility, and cell proliferation. Developmental-associated transcripts included those of the nervous system, muscle, skeleton, immune system, and organ morphogenesis.

In the combined analysis of the clinical specimens and the PPTP models, the rhabdomyosarcoma and rhabdoid tumor samples segregated into two groups. This separation is not based on alveolar versus embryonal subtype or site for rhabdoid tumors (central nervous system or kidney). The clinical NB samples also appeared to cluster in two separate groups, with the preclinical models segregating predominantly with one of these. The 12 neuroblastoma models profiled (xenografts and cell lines) are predominantly MYCN amplified (28), with the exceptions being CHLA-90, SK-N-AS, NB-EBc1, and CHLA-79. Hence, the groups do not segregate according to MYCN amplification status. However, the MYCN status of the

clinical samples used in this analysis, or whether samples were from treated or untreated patients, is unknown.

Differential expression between primary tumors and PPTP models. Although the PPTP models and primary tumors clustered predominantly by histotype, the xenograft samples tended to cluster within each histotype group (Fig. 2D). These observations prompted us to test for differences in expression between primary tumors and xenografts within the rhabdomyosarcoma, Ewing's sarcoma, and osteosarcoma histotypes, all of which have been analyzed on the HG-U133Plus2 array. For each histotype, we did a *t* test and identified probe sets with an estimated false discovery rate of <1.67% in each of the three comparisons. Overall, we identified 1,198 probe sets meeting this threshold and with >2-fold difference between primary and xenograft samples. By Gene Ontology analysis, the most significant biological functions enriched within the differentially expressed transcripts were those of immune response, cell cycle, RNA metabolism, and vesicle-mediated transport (Supplementary Table S4). Some examples of macrophage, B-cell, and vascular endothelial genes expressed 2.6- to 73.6-fold higher in primary tumor samples compared with PPTP models are shown in Table 1. This finding supports the observation that exclusion of immunosurveillance genes (based on gene annotations from Ingenuity Pathways) reduces the separation of rhabdomyosarcoma primary tumor samples from the PPTP models (Fig. 2D).

Analysis of genomic copy number change in the PPTP panel. DNA samples from 86 of the 87 PPTP panel were successfully analyzed using the Affymetrix 100K SNP assay. To identify regions of potential DNA gain or loss, the hybridization intensity of each SNP was normalized and compared with a diploid reference set using the dChipSNP software (25). Analysis of these samples identified recurrent regions of copy number gain and loss throughout the genome. The frequency of copy number alteration varied by location and by histotype (Fig. 3). For example, the PPTP osteosarcoma samples displayed recurrent copy number changes across almost the entire genome, whereas the leukemia and rhabdoid samples displayed the lowest frequency of copy number changes.

Table 1. Genes differentially expressed in clinical samples versus PPTP models

Tissue location	Gene	Tumor vs model (average fold change)
Macrophage	<i>CD14</i>	73.6
	<i>CD163</i>	58.9
	<i>CCR1</i>	9.6
	<i>CCR5</i>	9.3
	<i>CCL3</i>	8.6
	<i>CCL8</i>	8.1
	<i>IgK</i>	29.3
B cells Vascular/endothelial	<i>C1QA</i>	39.8
	<i>C5AR1</i>	39.8
	<i>EGFR</i>	22.8
	<i>ESAM</i>	3.3
	<i>FGFR1</i>	9.5
	<i>FLT1</i>	2.6
	<i>PDGFB</i>	8.8
	<i>PECAM1</i>	4.6
	<i>SELPLG</i>	15.9

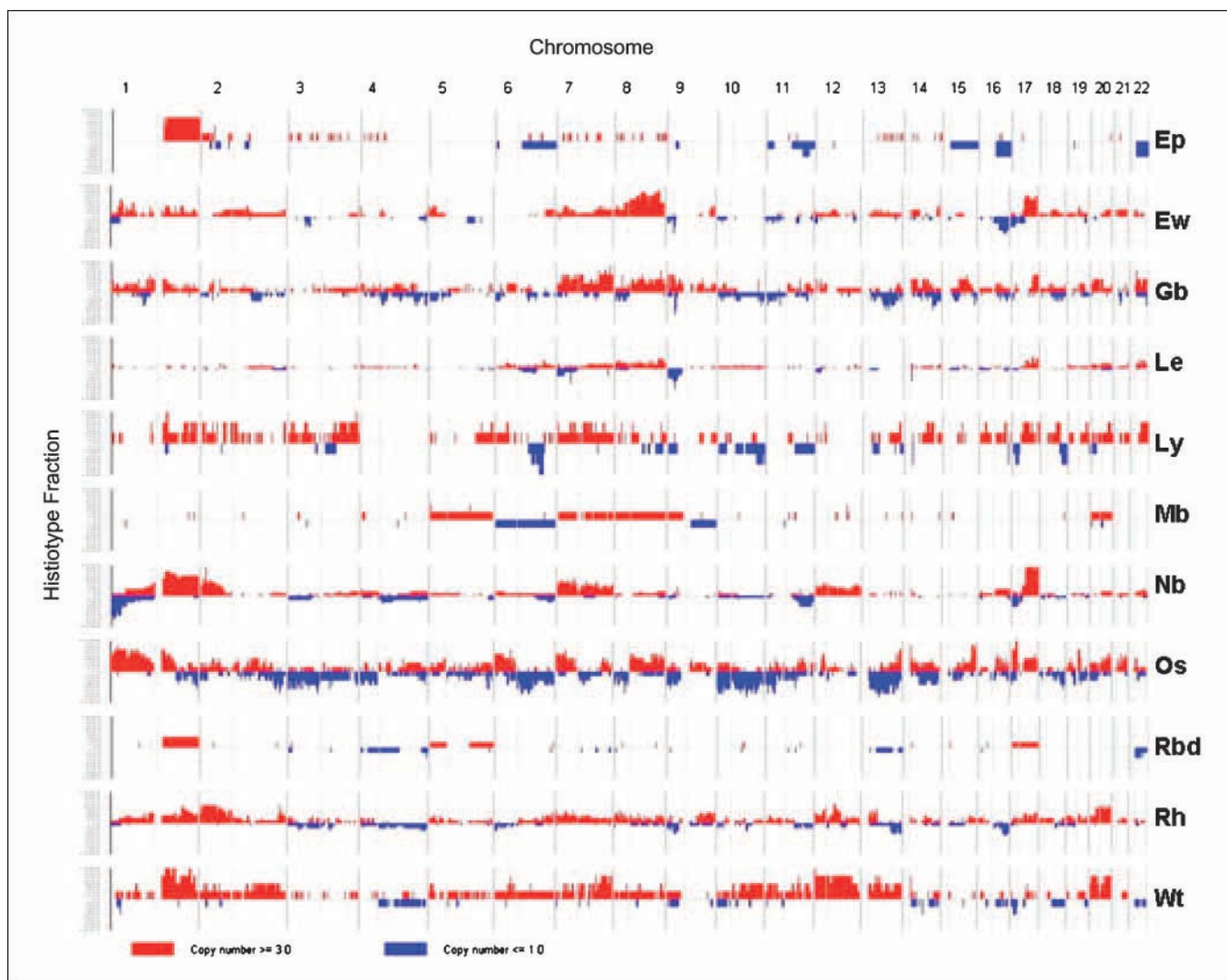


Fig. 3. Global assessment of DNA copy number change by SNP array. *Y axis*, fraction of samples within each tumor histotype with copy number amplification (*red*) or deletion (*blue*). SNP markers are ordered across the *X axis* according to their mapped positions from chromosome 1 to 22. *Vertical solid lines and dashed lines (gray)*, chromosome boundaries and centromeres, respectively. Tumor histotypes are displayed to the right of the plots. *Ep*, ependymoma; *Ew*, Ewing's sarcoma; *Gb*, glioblastoma; *Le*, leukemia; *Ly*, lymphoma; *Mb*, medulloblastoma; *Nb*, neuroblastoma; *Os*, osteosarcoma; *Rbd*, rhabdoid tumor; *Rh*, rhabdomyosarcoma; *Wt*, Wilms' tumor.

Using the copy number estimates from dChipSNP, we summarized recurrent genetic lesions across the PPTP panel (excluding osteosarcomas). Our criteria for "recurrent lesion" were a frequency of $\geq 50\%$ with DNA copy change ($3 \leq \text{DNA copy} \leq 1$) within at least one of the xenograft histotypes (Table 2; also Supplementary Table S5). Some of the genomic regions identified are consistent with previous reports. For example, deletion of 1p36 and amplification of 2p24 (*MYCN*) was common in neuroblastoma xenografts. This 2p24 region was also amplified in 7 of 12 rhabdomyosarcomas. Other gains and deletions were consistent with reports of clinical tumors of the appropriate histotype. For example, 3 of 4 ependymomas had gains at 1q21.3-q44 (29) and 7 of 9 Ewing's sarcoma samples had gains at 8q24.11-q24.21 (30). Deletions of 9p21, a region include the cyclin-dependent kinase inhibitors *CDKN2A* and *CDKN2B*, were frequent in Ewing's sarcoma (5 of 9), glioblastoma (5 of 7), and leukemia samples (11 of 16; Table 2; Supplementary Table S5).

Correlation of expression variation with genomic copy change in the PPTP panel. We used the combined copy number and expression data to identify genes whose expression might be altered by local genetic change during tumorigenesis. To perform this analysis, we identified SNP proximal to expression probe sets and tested whether DNA copy change was positively correlated with differential expression of nearby transcripts. We postulated the genes identified would be likely candidates as tumor suppressors or proto-oncogenes.

Of the 38,716 HG-U133Plus2 probe sets tested, 651 within the top-ranked 2% showed substantial correlation ($R \geq 0.6$, raw $P < 5.13 \times 10^{-10}$, Bonferroni-adjusted $P < 0.00002$) between DNA copy and gene expression (Fig. 4A). These 651 probe sets corresponded to 493 unique transcripts (Supplementary Table S6). The distribution of these transcripts across the genome did not correlate with chromosome length or with the number of genes per chromosome. After adjustment for chromosome length and the number of genes per

chromosome, three chromosome groupings were observed. The highest frequency of expression changes were observed on chromosomes 8, 17, and 22 (Fig. 4B). This nonrandom distribution of "hits" across the genome suggests selective disruption of genes within these regions during tumorigenesis. In addition to the unequal distribution of hits across the genome, there was also an unequal frequency of hits within each tumor histotype (Fig. 4C). For example, alterations on chromosome 12 were highest among Wilms' tumors, whereas the alterations on chromosome 8 were highest in Ewing's sarcoma. These observations are consistent with the patterns of global DNA copy change observed within each histotype (Fig. 3). Thus, the pattern of genetic alteration in the PPTP samples is not random; genes are disrupted in a histotype-specific manner, consistent with those known among their primary tumor counterparts. Eighty-five of the 493 unique transcripts mapped to 1 of the 26 areas of recurrent lesions listed in Table 2. The mapping of the transcripts correlated with copy number to the regions of recurrent gain or loss is provided in Supplementary Table S6. Approximately one-third of the 85 genes have functions related to cell proliferation, DNA repair, or cell death.

We explored the profiles of the copy-disrupted genes among the PPTP and primary tumor samples. Hierarchical clustering of the PPTP samples (including osteosarcoma) using the 651 HG-U133Plus2 probe sets showed strong correlation of expression that was related to tumor histotype (Fig. 5). Although some discrepancies were observed [e.g., the rhabdomyosarcoma split into two groups defined by p53 status (20), and two Ewing's sarcomas, two glioblastomas, and one medulloblastoma did not cluster with their other members], the majority of PPTP samples clustered according to histotype.

Discussion

We reported previously the similarity in expression profiles for selected childhood tumor models and their clinical counterparts as defined by cDNA profiling. The current study advances the previous analysis in several ways. We used an expanded gene probe set, and the results from the models were contrasted to a completely different set of human biopsies than those used in the previous work. It excluded several tumors of murine origin that were "accepted" by cDNA profiling and identified several osteosarcoma cell lines that had expression profiles that were distinct from clinical osteosarcoma and from osteosarcoma xenografts. Further, as comparing results using these two platforms is very complex, the current data set presents results that can readily be compared with other data sets obtained using the Affymetrix technology, which includes the majority of clinical results published for childhood cancer.

Hierarchical clustering of cell lines and xenograft samples separated the PPTP panel into discrete clusters whose members were almost exclusively based on histotype, with only three exceptions. Similarly, expression profiling showed that seven of the eight histotypes with matching clinical tumor-xenograft pairs cosegregated in the same cluster, with the rhabdomyosarcomas being the single outlier. However, if either leukemia samples or genes associated with immunosurveillance were removed and then profiles were reclustered with variable genes, then all (with three exceptions) histotype samples cosegregated (Fig. 2D).

Although the models generally segregated with their clinical histologies, there are significant differences in expression profiles of xenografts and their respective clinical tumors. For

Table 2. Recurrent gene lesions

Cytoband	Start (Mb)	End (Mb)	Size (Mb)	Ependymoma (n = 4)	Ewing's sarcoma (n = 9)	Glioblastoma (n = 7)	Leukemia (n = 16)
Amplifications							
1q21.3-q44	150.034	245.12	95.086	3	1	1	0
2p25.1	10.062	11.645	1.583	1	0	0	2
2p24.3	15.72	16.465	0.745	1	0	0	0
2p24.2-p16.1	16.873	60.356	43.483	0	0	0	0
2p14	64.333	65.547	1.214	0	1	1	2
3q27.2-q27.3	18.696	18.818	0.122	0	1	1	1
7p21.1-p11.2	13.986	54.398	40.412	1	2	4	1
7q31.31-q35	117.011	147.281	30.27	1	1	4	2
8q11.21-q22.3	48.151	106.195	58.044	0	6	3	2
8q24.11-q24.21	117.746	128.809	11.063	1	7	3	4
9p22.3-p22.2	14.438	17.312	2.874	0	0	4	0
12p13.33-p12.1	10.76	26.234	15.474	0	1	2	0
12q14.1-q15	56.263	69.037	12.774	0	2	1	0
13q14.11	39.703	40.042	0.339	0	0	2	0
14q11.2	21.703	22.061	0.358	1	2	3	3
15q22.31-q23	64.63	66.673	2.043	0	0	4	1
17q21.31-q25.3	41.159	78.182	37.023	0	6	4	3
20p12.2-p12.1	9.002	17.491	8.489	0	0	3	1
20q11.23-q13.33	33.909	62.377	28.468	0	2	1	2
21q22.3	45.112	46.015	0.903	0	2	0	3
22q11.21	17.722	17.723	0.001	0	2	5	2
Deletions							
1p36.32-p36.11	3.118	5.001	1.883	0	2	0	0
6q22.31-q22.33	121.263	130.387	9.124	1	0	0	0
9p21.3	21.675	22.538	0.863	1	5	5	11
14q11.2	21.942	22.033	0.091	0	0	0	8
16q22.3	72.413	73.507	1.094	2	5	2	1

example, many cell cycle genes including the cyclins CCNA2 and CCNE2, the cyclin-dependent kinases CDK3 and CDK4, and the mitotic checkpoint genes BUB3 and CHEK1 were expressed 3- to 5-fold lower in primary samples compared with xenograft samples. Further, BCL2 was expressed ~ 5-fold higher in primary samples compared with tumor models, which could be related to either infiltrating stromal and immune cells in primary samples or differences in Bcl-2 gene expression in tumor cells from clinical samples. Many expression differences between clinical samples and the preclinical models appear to arise from nontumor cells present in the former but absent in xenograft models. The differential expression of immune-related genes provides support for this notion. For example, many macrophage-associated markers as well as those of B cells had 8- to 73-fold higher expression levels in primary tumors (Table 1). Further, many endothelial and vascular gene profiles (Table 2) were expressed at 10- to 30-fold greater levels in primary tumors than in xenografts. As anticipated, expression of all HLA genes was decreased in xenografts compared with tumor biopsies (3- to 125-fold; data not shown). Thus, the most significant differences in expression between primary tumors and PPTP models are associated with immune and endothelial cell functions.

Studies of childhood cancer using cytogenetic analysis or more contemporary molecular approaches such as comparative genomic hybridization or fluorescence *in situ* hybridization have revealed gains and losses of DNA that appear characteristic for a particular histotype. However, similar analyses for models derived from childhood cancers have not been extensively reported. SNP analysis revealed specific changes in copy number in PPTP models that are consistent with gains and

losses of DNA in clinical tumor samples. For example, 1q gain, 6q loss, and loss of chromosome 22 are common aberrations in ependymoma (31), and these alterations are recapitulated in the xenografts ($n = 4$) within the PPTP panel. Common abnormalities in clinical samples for high-risk neuroblastoma include gains of 17q and 1q as well as 1p loss and 11q loss, and the SNP analysis of neuroblastoma xenografts ($n = 14$) recapitulate these clinical findings (32–37). Interestingly, rhabdoid tumor xenografts ($n = 6$) showed the fewest changes in copy number. The most frequent change found in 2 of 6 models was in chromosome 22q where loss of copy number was detected, consistent with clinical reports (38, 39). Each of the Ewing's sarcoma xenografts ($n = 9$) shows the t(11:22) translocation resulting in expression of EWS/FLI1 or EWS/ERG transcripts (27), and SNP analysis additionally revealed increased copy number at 8q and 17q and loss of copy number on 16q. Chromosome gains of 1q, 8, and 12 have been reported for clinical specimens of Ewing's sarcoma (40), and gains of chromosome 17 have been detected by comparative genomic hybridization (30). The gains and losses of DNA for the Wilms' xenograft samples ($n = 4$; 1q, 2q, 12, and 20 gains and 4q, 16q, and 18q losses) are highly consistent with array comparative genomic hybridization analysis of favorable histology Wilms' tumors (41). Of note, gain of 1q has been correlated with poor outcome in children with Wilms' tumor as have loss of heterozygosity at 1p and 16q (42, 43). The SNP analysis for glioblastoma models ($n = 7$) is also consistent with genomic profiling of clinical samples with increases of chromosome 7 and loss of genetic material on 4q and 13q (44). One difference is the gain of genetic material at 8q in the models, whereas losses at both 8p and 8q were more frequent

Table 2. Recurrent gene lesions (Cont'd)

Lymphoma ($n = 3$)	Medulloblastoma ($n = 4$)	Neuroblastoma ($n = 14$)	Osteosarcoma ($n = 7$)	Rhabdoid ($n = 6$)	Rhabdomyosarcoma ($n = 12$)	Wilms' tumor ($n = 4$)	Total ($n = 86$)
1	0	10	3	2	6	3	30
1	0	8	1	0	7	1	21
0	0	13	1	0	7	1	23
0	0	6	2	0	7	1	16
3	0	2	1	0	5	1	16
3	0	2	0	0	1	1	10
2	1	8	5	0	4	1	29
1	1	4	2	0	2	3	21
1	1	1	3	0	1	1	19
0	1	2	3	0	3	0	24
0	1	2	1	0	2	1	11
0	0	6	3	0	4	3	19
0	0	4	1	0	5	3	16
0	0	0	0	0	6	2	10
1	2	3	6	1	3	3	28
0	0	0	2	0	1	0	8
2	0	13	3	1	3	1	36
0	1	0	2	0	2	3	12
1	1	2	4	0	7	3	23
3	0	1	5	0	1	1	16
0	0	2	3	0	1	0	15
0	0	11	0	0	1	1	15
3	0	2	2	0	1	0	9
1	0	1	3	0	2	1	30
2	0	0	0	0	0	0	10
0	0	0	1	0	4	0	15

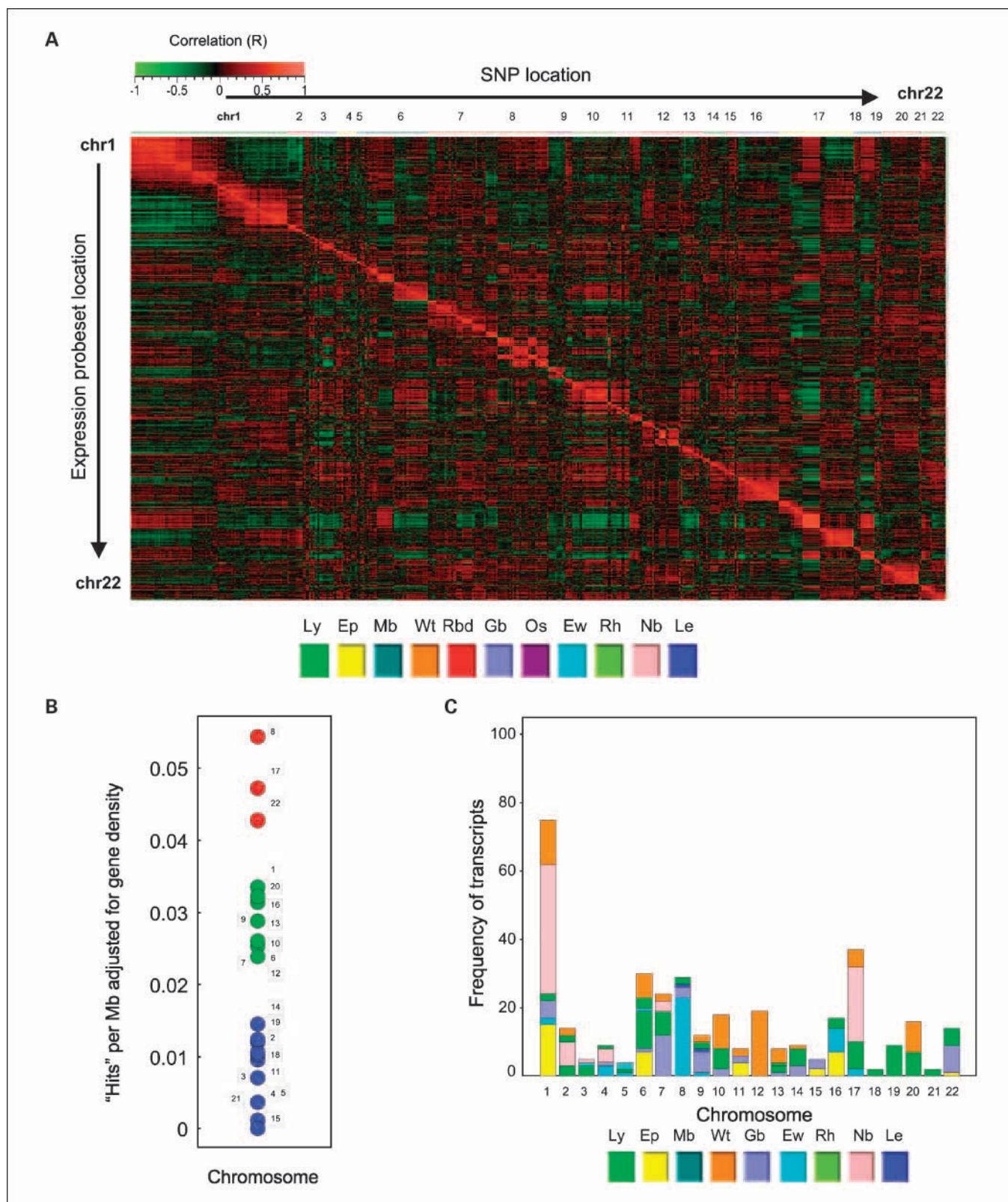


Fig. 4. Correlation of DNA copy and expression across the PPTP samples. *A*, correlation of expression variation and DNA copy variation according to genomic location. SNP markers are ordered across the *X axis*, whereas expression probe sets are ordered on the *Y axis* according to their mapped positions. The heat map displays Pearson's coefficient (*R*) of the association between copy change and relative expression. Results from the 493 unique transcripts with $R \geq 0.6$. *B*, distribution of the 493 copy-disrupted transcripts ($R \geq 0.6$) across the genome. *Y axis*, frequency of observations after adjustment for chromosome length and number of genes per chromosome. Chromosomes are labeled by number and colored by their apparent grouping. *C*, distribution of the 493 copy-disrupted transcripts according to genome location and frequency of observation in tumor histotypes. The number of transcripts is plotted (*Y axis*) against chromosome position (*X axis*). Colors within the bars indicate the tumor histotype with the most frequent number of changes at a given chromosome location.

Table 3. Regions identified that contain genes with known alterations in human cancer

Region	Genes
Amplifications	
1q21-q44	<i>ABL2, FCGR2B, FH, HRPT2, IRTA1, PBX1, SDHC, TPR</i>
2p24	<i>MYCN</i>
2p24-p16	<i>ALK, BCL11A, MSH2, MSH6</i>
3q27-q27	<i>EIF4A2</i>
7p21-p11	<i>HOXA13, JAZF1, ZNFN1A1</i>
7q31-q35	<i>BRAF, TIF1</i>
8q11-q22	<i>NBS1, NCOA2, PLAG1</i>
8q24-q24	<i>EXT1</i>
12p13-p12	<i>HIST1H4I, CCND2, ETV6, KRAS</i>
12q14-q15	<i>HMGA2</i>
13q14	<i>FOXO1A</i>
14q11	<i>TCR-α</i>
17q21-q25	<i>BRIP1, CLTC, COL1A1, HLF, MSI2, PRKAR1A</i>
20q11-q13	<i>GNAS</i>
Deletions	
1p36-p36	<i>PAX7, PRDM16</i>
9p21	<i>CDKN2A/2B</i>
14q11	<i>TCR-α</i>

amplification of MYCN, particularly in alveolar rhabdomyosarcoma (47–49).

Approximately one-third of the regions with recurrent copy change in the PPTP models do not contain genes with known alterations in human cancer. One example is gain at 22q11.21, which was observed in 5 of 7 glioblastoma samples and 15 of 86 PPTP models. Another example of tumor-associated copy change is loss at 16q22.3, which was observed in 5 of 9 Ewing's sarcoma and 4 of 12 rhabdomyosarcoma PPTP models. This deleted region contains four transcripts (C16orf47, FA2H, GLG1, and PSMD7) that show strong correlation of expression with copy number. Of the four candidate genes, GLG1 and PSMD7 have roles in protein metabolism and protein turnover, respectively. GLG1 also binds basic fibroblast growth factor; thus, loss of GLG1 in tumor cells may modify the fibroblast growth factor signaling pathway. Amplification at 21q22.3 in 5 of 7 osteosarcoma models may also influence fibroblast growth factor signaling. This region contains 7 candidate loci. One gene is PTTG1IP. The PTTG1IP gene product binds PTTG1, thus causing its translocation from the cytoplasm to the nucleus where PTTG1 activates expression of basic fibroblast growth

factor-2. PTTG1 has transforming activity *in vitro* and tumorigenic activity *in vivo*, and the gene is highly expressed in various tumors (reviewed by ref. 50).

In tumor samples representing 11 different histotypes, we identified 493 transcripts whose differential expression was highly correlated with DNA copy change, of which only 5 are common to the profiles selected in Fig. 1. Our results show that these genes whose expression is altered by proximal DNA copy number changes have a strong histotype pattern within the PPTP. Thus, two observations can be made. First, most of the histotype-specific DNA lesions identified also contain genes whose expression correlates with genomic copy number change. Second, these findings point to a subset of genes whose altered expression is likely important to tumorigenesis within a given histotype and thereby potentially important targets for small-molecule therapeutics. However, confirmation of these results will require analysis of extended cohorts of models within a histotype.

The molecularly characterized PPTP panel offers a unique resource for relating the effect of novel therapeutic interventions to the underlying biological factors in tumors that determine response. The gene expression data set may provide information relevant to the primary cellular targets of novel agents, and it also may allow identification of roles for previously unsuspected genes in affecting response to treatment. The gene copy number data for the PPTP panel are likely to be increasingly relevant to therapeutics development as evidenced by the identification of genomic abnormalities associated with the response of adult cancers to molecularly targeted agents (e.g., epidermal growth factor receptor mutation for erlotinib, HER-2 amplification for trastuzumab, and Bcl-2 amplification for ABT-263). The comprehensive genomic analysis described in this report and to be deposited in a public database¹⁷ will serve as a reference point for researchers interested in the treatment of childhood cancers. These analyses enhance the value of the PPTP preclinical models as a unique resource that encompasses a substantial proportion of the genomic diversity of childhood cancers.

Disclosure of Potential Conflicts of Interest

No potential conflicts of interest were disclosed.

¹⁷ <http://pptp.stjude.org/>

References

- Ries LA, Eisner MP, Kosary CL, et al. SEER cancer statistics review 1975-2002. Bethesda, MD: National Cancer Institute, 2005.
- Bachmann PS, Gorman R, Mackenzie KL, Lutze-Mann L, Lock RB. Dexamethasone resistance in B-cell precursor childhood acute lymphoblastic leukemia occurs downstream of ligand-induced nuclear translocation of the glucocorticoid receptor. *Blood* 2005; 105:2519–26.
- Houghton PJ, Adamson PC, Blaney S, et al. Testing of new agents in childhood cancer preclinical models: meeting summary. *Clin Cancer Res* 2002;8:3646–57.
- Geist MJ, Maris DO, Grady MS. Blood-brain barrier permeability is not altered by allograft or xenograft fetal neural cell suspension grafts. *Exp Neurol* 1991;111: 166–74.
- Schold SC, Jr., Friedman HS. Human brain tumor xenografts. *Prog Exp Tumor Res* 1984;28:18–31.
- Fuchs HE, Archer GE, Colvin OM, et al. Activity of intrathecal 4-hydroperoxycyclophosphamide in a nude rat model of human neoplastic meningitis. *Cancer Res* 1990;50:1954–9.
- Friedman HS, Burger PC, Bigner SH, et al. Phenotypic and genotypic analysis of a human medulloblastoma cell line and transplantable xenograft (D341 Med) demonstrating amplification of c-myc. *Am J Pathol* 1988;130:472–84.
- Friedman HS, Colvin OM, Ludeman SM, et al. Experimental chemotherapy of human medulloblastoma with classical alkylators. *Cancer Res* 1986;46: 2827–33.
- Friedman HS, Houghton PJ, Schold SC, Keir S, Bigner DD. Activity of 9-dimethylaminomethyl-10-hydroxycamptothecin against pediatric and adult central nervous system tumor xenografts. *Cancer Chemother Pharmacol* 1994;34:171–4.
- Friedman HS, Keir ST, Houghton PJ, Lawless AA, Bigner DD, Waters SJ. Activity of iriflufen (6-hydroxymethylacetylfulvene) in the treatment of glioblastoma multiforme-derived xenografts in athymic mice. *Cancer Chemother Pharmacol* 2001;48:413–6.
- Liem NL, Papa RA, Milross CG, et al. Characteriza-

- tion of childhood acute lymphoblastic leukemia xenograft models for the preclinical evaluation of new therapies. *Blood* 2004;103:3905–14.
12. Shusterman S, Grupp SA, Barr R, Carpentieri D, Zhao H, Maris JM. The angiogenesis inhibitor tnp-470 effectively inhibits human neuroblastoma xenograft growth, especially in the setting of subclinical disease. *Clin Cancer Res* 2001;7:977–84.
 13. Vassal G, Boland I, Santos A, et al. Potent therapeutic activity of irinotecan (CPT-11) and its schedule dependency in medulloblastoma xenografts in nude mice. *Int J Cancer* 1997;73:156–63.
 14. Vassal G, Merlin JL, Terrier-Lacombe MJ, et al. *In vivo* antitumor activity of S16020, a topoisomerase II inhibitor, and doxorubicin against human brain tumor xenografts. *Cancer Chemother Pharmacol* 2003;51:385–94.
 15. Middlemas DS, Stewart CF, Kirstein MN, et al. Biochemical correlates of temozolomide sensitivity in pediatric solid tumor xenograft models. *Clin Cancer Res* 2000;6:998–1007.
 16. Mintz MB, Sowers R, Brown KM, et al. An expression signature classifies chemotherapy-resistant pediatric osteosarcoma. *Cancer Res* 2005;65:1748–54.
 17. Jaboin J, Wild J, Hamidi H, et al. MS-27-275, an inhibitor of histone deacetylase, has marked *in vitro* and *in vivo* antitumor activity against pediatric solid tumors. *Cancer Res* 2002;62:6108–15.
 18. Peterson JK, Houghton PJ. Integrating pharmacology and *in vivo* cancer models in preclinical and clinical drug development. *Eur J Cancer* 2004;40:837–44.
 19. Whiteford CC, Bilke S, Greer BT, et al. Credentialing preclinical pediatric xenograft models using gene expression and tissue microarray analysis. *Cancer Res* 2007;67:32–40.
 20. Houghton PJ, Morton CL, Tucker C, et al. The Pediatric Preclinical Testing Program: description of models and early testing results. *Pediatr Blood Cancer* 2007;49:928–40.
 21. Ross ME, Zhou X, Song G, et al. Classification of pediatric acute lymphoblastic leukemia by gene expression profiling. *Blood* 2003;102:2951–9.
 22. Taylor MD, Poppleton H, Fuller C, et al. Radial glia cells are candidate stem cells of ependymoma. *Cancer Cell* 2005;8:323–35.
 23. Thompson MC, Fuller C, Hogg TL, et al. Genomics identifies medulloblastoma subgroups that are enriched for specific genetic alterations. *J Clin Oncol* 2006;24:1924–31.
 24. Benjamini Y, Hochberg Y. Controlling the false discovery rate: a practical and powerful approach to multiple testing. *J R Stat Soc B* 1995;57:289–300.
 25. Lieberfarb ME, Lin M, Lechpammer M, et al. Genome-wide loss of heterozygosity analysis from laser capture microdissected prostate cancer using single nucleotide polymorphic allele (SNP) arrays and a novel bioinformatics platform dChipSNP. *Cancer Res* 2003;63:4781–5.
 26. Li C, Wong WH. Model-based analysis of oligonucleotide arrays: expression index computation and outlier detection. *Proc Natl Acad Sci U S A* 2001;98:31–6.
 27. Smith MA, Morton CL, Phelps D, Girtman K, Neale G, Houghton PJ. SK-NEP-1 and Rh1 are Ewing family tumor lines. *Pediatr Blood Cancer* 2008;50:703–6.
 28. Houghton PJ, Morton CL, Tucker C, et al. The Pediatric Preclinical Testing Program: description of models and early testing results. *Pediatr Blood Cancer* 2007;49:928–40.
 29. Mendrzyk F, Korshunov A, Benner A, et al. Identification of gains on 1q and epidermal growth factor receptor overexpression as independent prognostic markers in intracranial ependymoma. *Clin Cancer Res* 2006;12:2070–9.
 30. Tarkkanen M, Kiuru-Kuhlefelt S, Blomqvist C, et al. Clinical correlations of genetic changes by comparative genomic hybridization in Ewing sarcoma and related tumors. *Cancer Genet Cytogenet* 1999;114:35–41.
 31. Ward S, Harding B, Wilkins P, et al. Gain of 1q and loss of 22 are the most common changes detected by comparative genomic hybridisation in paediatric ependymoma. *Genes Chromosomes Cancer* 2001;32:59–66.
 32. Trakhtenbrot L, Cohen N, Betts DR, et al. Interphase fluorescence *in situ* hybridization detection of chromosome 17 and 17q region gains in neuroblastoma: are they secondary events? *Cancer Genet Cytogenet* 2002;137:95–101.
 33. Maris JM, Guo C, White PS, et al. Allelic deletion at chromosome bands 11q14-23 is common in neuroblastoma. *Med Pediatr Oncol* 2001;36:24–7.
 34. Brinkschmidt C, Christiansen H, Terpe HJ, et al. Distal chromosome 17 gains in neuroblastomas detected by comparative genomic hybridization (CGH) are associated with a poor clinical outcome. *Med Pediatr Oncol* 2001;36:11–3.
 35. Brinkschmidt C, Christiansen H, Terpe HJ, et al. Comparative genomic hybridization (CGH) analysis of neuroblastomas—an important methodological approach in paediatric tumour pathology. *J Pathol* 1997;181:394–400.
 36. Hirai M, Yoshida S, Kashiwagi H, et al. 1q23 gain is associated with progressive neuroblastoma resistant to aggressive treatment. *Genes Chromosomes Cancer* 1999;25:261–9.
 37. Van Gele M, Van Roy N, Jauch A, et al. Sensitive and reliable detection of genomic imbalances in human neuroblastomas using comparative genomic hybridisation analysis. *Eur J Cancer* 1997;33:1979–82.
 38. Wieser R, Fritz B, Ullmann R, et al. Novel rearrangement of chromosome band 22q11.2 causing 22q11 microdeletion syndrome-like phenotype and rhabdoid tumor of the kidney. *Hum Mutat* 2005;26:78–83.
 39. Raisanen J, Biegel JA, Hatanpaa KJ, Judkins A, White CL, Perry A. Chromosome 22q deletions in atypical teratoid/rhabdoid tumors in adults. *Brain Pathol* 2005;15:23–8.
 40. Maurici D, Perez-Atayde A, Grier HE, Baldini N, Serra M, Fletcher JA. Frequency and implications of chromosome 8 and 12 gains in Ewing sarcoma. *Cancer Genet Cytogenet* 1998;100:106–10.
 41. Natrajan R, Williams RD, Hing SN, et al. Array CGH profiling of favourable histology Wilms tumours reveals novel gains and losses associated with relapse. *J Pathol* 2006;210:49–58.
 42. Grundy PE, Telzerow PE, Breslow N, Moksness J, Huff V, Paterson MC. Loss of heterozygosity for chromosomes 16q and 1p in Wilms' tumors predicts an adverse outcome. *Cancer Res* 1994;54:2331–3.
 43. Grundy PE, Breslow NE, Li S, et al. Loss of heterozygosity for chromosomes 1p and 16q is an adverse prognostic factor in favorable-histology Wilms tumor: a report from the National Wilms Tumor Study Group. *J Clin Oncol* 2005;23:7312–21.
 44. Mulholland PJ, Fiegler H, Mazzanti C, et al. Genomic profiling identifies discrete deletions associated with translocations in glioblastoma multiforme. *Cell Cycle* 2006;5:783–91.
 45. Bridge JA, Nelson M, McComb E, et al. Cytogenetic findings in 73 osteosarcoma specimens and a review of the literature. *Cancer Genet Cytogenet* 1997;95:74–87.
 46. Futreal PA, Coin L, Marshall M, et al. A census of human cancer genes. *Nat Rev Cancer* 2004;4:177–83.
 47. Driman D, Thorner PS, Greenberg ML, Chilton-MacNeill S, Squire J. MYCN gene amplification in rhabdomyosarcoma. *Cancer* 1994;73:2231–7.
 48. Hachitanda Y, Toyoshima S, Akazawa K, Tsuneyoshi M. N-myc gene amplification in rhabdomyosarcoma detected by fluorescence *in situ* hybridization: its correlation with histologic features. *Mod Pathol* 1998;11:1222–7.
 49. Williamson D, Lu YJ, Gordon T, et al. Relationship between MYCN copy number and expression in rhabdomyosarcomas and correlation with adverse prognosis in the alveolar subtype. *J Clin Oncol* 2005;23:880–8.
 50. Tfelt-Hansen J, Kanuparthi D, Chattopadhyay N. The emerging role of pituitary tumor transforming gene in tumorigenesis. *Clin Med Res* 2006;4:130–7.